

# Dynamics and Thermodynamics of a Novel Phase of $\text{NaAlH}_4$

Brandon C. Wood\* and Nicola Marzari

*Department of Materials Science and Engineering,*

*Massachusetts Institute of Technology, Cambridge, MA 02139*

## Abstract

We characterize a novel orthorhombic phase ( $\gamma$ ) of  $\text{NaAlH}_4$ , discovered using first-principles molecular dynamics, and discuss its relevance to the dehydrogenation mechanism. This phase is close in energy to the known low-temperature structure and becomes the stabler phase above 320 K, thanks to a larger vibrational entropy associated with  $\text{AlH}_4$  rotational modes. The structural similarity of  $\gamma$ - $\text{NaAlH}_4$  to  $\alpha$ - $\text{Na}_3\text{AlH}_6$  suggests it acts as a key intermediate during hydrogen release. Findings are consistent with recent experiments recording an unknown phase during dehydrogenation.

PACS numbers: 71.15.Pd, 66.30.-h, 66.30.Dn

---

\* Present address: Lawrence Livermore National Laboratory, Livermore, CA 94550

Complex light-metal hydrides represent a materials solution to the hydrogen-storage problem [1] because of their potential for acceptably high gravimetric capacities, as well as an ability to be engineered for favorable hydrogen release kinetics. Of these, sodium alanate ( $\text{NaAlH}_4$ ) has attracted particular interest by combining relatively high theoretical hydrogen release with ready reversibility through the addition of transition metal dopants [2, 3]. As such, the material has been widely studied as a template for developing novel hydrogen storage solutions. Several recent first-principles studies [4, 5, 6, 7, 8, 9, 10, 11, 12, 13, 14, 15, 16, 17, 18, 19, 20] have addressed the structure and thermodynamics of the sodium alanate system. Nevertheless, important questions regarding the precise mechanism of dehydrogenation and the nature of the key phase transition from  $\text{NaAlH}_4$  to  $\text{Na}_3\text{AlH}_6$  remain unanswered.

In this Letter, we present static, linear-response, and molecular dynamics (MD) calculations based on density-functional theory (DFT) that support the existence of a hitherto unknown orthorhombic phase of  $\text{NaAlH}_4$  ( $\gamma$ ), found to be thermodynamically favored over the low-temperature  $\alpha$  phase at relevant operating temperatures for dehydrogenation. This phase is entropically stabilized by activation of  $\text{AlH}_4$  rotation and readily nucleates in MD simulations of (001) surface slabs. Our evidence is presented alongside recent experiments to highlight the likely significance of this phase in stabilizing and mediating the decomposition reaction.

Our calculations are based on DFT in the plane-wave pseudopotential formalism [21] using the PBE exchange-correlation functional [22]. Ultrasoft pseudopotentials [23] for Na ( $2s^2 2p^6 3s^{0.5}$ ), H, and Al ( $3s^2 3p^2$ ) were taken from the Quantum-Espresso distribution [21]. A second Troullier-Martins pseudopotential [24] for Na, used only for the MD runs, was generated in a  $3s^{0.5} 3p^{0.05}$  valence configuration, with nonlinear core corrections [25] added. For the MD simulations, cutoffs of 25 and 200 Ry were used for the wavefunctions and charge density, respectively, representing convergence of forces to within 0.02 eV/Å. These were raised to 30 and 300 Ry for the total-energy and linear-response calculations. The  $\alpha \rightarrow \gamma$  transition was studied using Car-Parrinello MD simulations [26] of bulk supercells of  $\text{NaAlH}_4$  with 96 atoms ( $2 \times 2 \times 1$   $\alpha$  unit cells) and of slab supercells with 192 atoms (8 layers;  $2 \times 2 \times 2$   $\alpha$  unit cells). Slabs were cleaved along the (001) plane—verified experimentally and theoretically as the stablest facet [14]—with 14 Å of vacuum inserted between images. Except where indicated, slab simulations were performed in the  $NVT$  ensemble, whereas

bulk simulations were performed in the  $NPT$  ensemble at zero pressure using the Parrinello-Rahman extended Lagrangian formalism [27]. The theoretical  $\alpha$  lattice parameter was used for the initial cell state. Bulk  $\text{NaAlH}_4$  was sampled at 50 K intervals from 300–650 K; surface slabs at 25 K intervals from 225–425 K. Temperatures were maintained using Nosé-Hoover chains [28], with electronic fictitious mass  $\mu = 500$  au and  $\Delta t = 6$  au. Following 5 ps of thermalization, each bulk simulation ran for 25 ps and each surface simulation for 15 ps.

The new phase, designated throughout this Letter as  $\gamma$  to distinguish it from the high-pressure  $\beta$  phase [29], manifests itself in our MD simulations of the (001) surface slab of  $\text{NaAlH}_4$ . Specifically, we find that the (001) slab exhibits a spontaneous transition from the  $\alpha$  to the  $\gamma$  phase for  $250 < T < 350$  K, within 15 ps into the production run. This transition is clearly visible in Fig. 1a, which compares final configurations of the surface slab at select simulation temperatures. (Melting occurred above 350 K; tendency to melt is enhanced by our finite slab thickness). To rule out finite-size or supercell restrictions, we ran additional surface simulations at 300 K, one with a larger 270-atom supercell and one in the  $NPT$  ensemble. Both evidenced the same transition to the  $\gamma$  phase. An  $NPT$  simulation of bulk  $\gamma\text{-NaAlH}_4$  at 300 K was also performed, with the new phase remaining stable throughout the run.

Figure 1b illustrates the basic structural differences between the  $\alpha$  and  $\gamma$  phases, as observed in the slab simulations. Three qualitative features of the  $\alpha \rightarrow \gamma$  transition emerge in the MD runs: a rotational disordering of the  $\text{AlH}_4$  groups; an expansion of the crystal along  $\hat{\mathbf{c}}$ ; and a shear of successive crystal planes parallel to the surface, generating the lattice symmetry of the  $\gamma$  phase.

In contrast to the surface slab, no structural reorganization was observed in  $NPT$  simulations of bulk  $\text{NaAlH}_4$  (until melting at  $T \geq 550$  K). Given its facile expression in the (001) slab, we conclude that any observation of the transition to  $\gamma$  in the bulk must be kinetically hindered, requiring much longer simulations for observation. This hindrance relates to the volume expansion of the lattice during the transition, as discussed further below.

In Fig. 2, we present the structure of  $\gamma\text{-NaAlH}_4$ , taken from representative dynamics timesteps and relaxed with respect to all internal parameters and lattice vectors. The unit cell is best described as a 12-atom base-centered orthorhombic (bco) structure with space group  $Pmmn$  and  $a = 6.500$  Å,  $b = 7.105$  Å, and  $c = 7.072$  Å (see Table I for details; note the near-degeneracy of  $b$  and  $c$ ). We compared the energy of this structure, calculated using

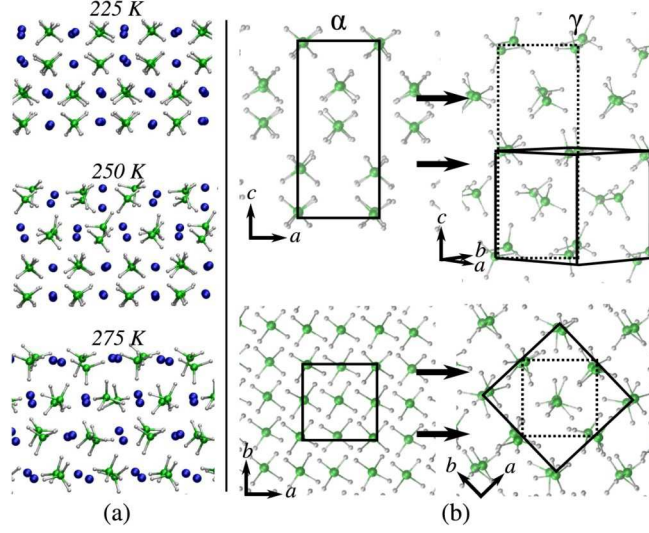


FIG. 1: (Color online) (a) Equilibrated structure of an 8-layer (001) surface slab of NaAlH<sub>4</sub> taken from MD runs at 225, 250, and 275 K (topmost four layers shown). Na/Al/H atoms are shown in blue/green/white. Slabs are viewed along the  $\hat{b}$  axis of the  $\alpha$  phase, with  $\hat{c}$  oriented upwards. Surface shear at 250 K signals the onset of  $\gamma$ , complete by 275 K. (b) Schematic illustration of structural differences before (left) and after (right) the transition (identical viewpoints, Na atoms omitted). Solid lines outline the  $\alpha$  and  $\gamma$  unit cells; dotted lines connect original boundary atoms of the  $\alpha$  cell.

216  $\mathbf{k}$ -points in the full Brillouin Zone, to that of the low-temperature  $\alpha$  phase, calculated using a 324- $\mathbf{k}$  point mesh of similar density. At 0 K, the  $\alpha$  phase is lower in energy by only 9 meV/atom, pointing to a close competition for stability between these two phases. The accuracy of the PBE energetics was also checked against quantum-chemistry calculations on isolated 72-atom clusters of  $\alpha$ - and  $\gamma$ -NaAlH<sub>4</sub> using the B3LYP functional and a 6-311+G basis; the difference between B3LYP and PBE in the relative stability of the two clusters (likely bracketing the exact result) was 2 meV/atom.

A comparison of Figs. 1 and 2 reveals differences between the  $\gamma$  phase at finite temperature and its zero-temperature, fully relaxed equivalent. The zero-temperature structure features alignment of H (but not Al) in successive AlH<sub>4</sub> tetrahedra along  $\hat{c}$ . At finite temperatures,  $\gamma$ -NaAlH<sub>4</sub> instead exhibits an average alignment of Al along  $\hat{c}$ , a consequence of randomized AlH<sub>4</sub> orientations and increased configurational freedom.

To establish finite-temperature properties, we have calculated the phonons [30] and

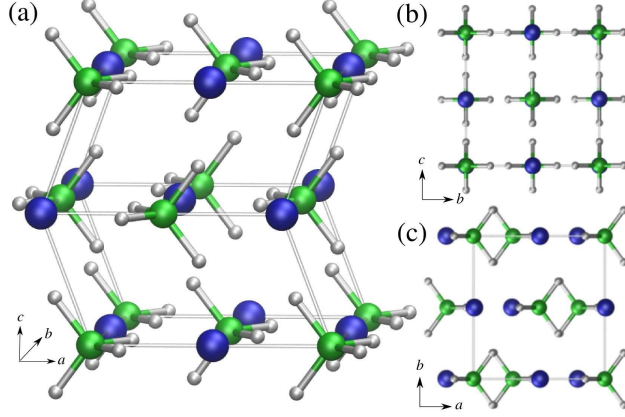


FIG. 2: (Color online) Structure of orthorhombic  $\gamma$ -NaAlH<sub>4</sub>, shown (a) in the standard view; (b) along  $\hat{\mathbf{a}}$ ; and (c) along  $\hat{\mathbf{c}}$ . The color scheme follows Fig. 1.

TABLE I: Internal atomic positions for  $\gamma$ -NaAlH<sub>4</sub> ( $Pmmn$ ;  $a = 6.500$  Å,  $b = 7.105$  Å,  $c = 7.072$  Å). Units are fractional coordinates ( $\alpha, \beta, \gamma$ ) of the primitive bco lattice vectors.

Atom type	$\alpha$	$\beta$	$\gamma$
Na	$\pm 0.141$	$\mp 0.141$	$\pm 0.250$
Al	$\pm 0.349$	$\mp 0.349$	$\mp 0.250$
H	$\pm 0.198$	$\mp 0.198$	$\mp 0.067$
H	$\pm 0.198$	$\mp 0.198$	$\mp 0.433$
H	$\pm 0.313$	$\pm 0.317$	$\mp 0.250$
H	$\pm 0.317$	$\pm 0.313$	$\pm 0.250$

phonon density of states (PDOS) for the  $\alpha$  and  $\gamma$  phases using density-functional perturbation theory [31]. Figure 3 compares the PDOS for  $\alpha$ -NaAlH<sub>4</sub> (in close agreement with Ref. 16) with  $\gamma$ -NaAlH<sub>4</sub>. Bands below  $180 \text{ cm}^{-1}$  are Na/Al translational lattice modes;  $180$ – $580 \text{ cm}^{-1}$ , AlH<sub>4</sub> rotational modes;  $750$ – $900 \text{ cm}^{-1}$ , bending modes; and above  $1600 \text{ cm}^{-1}$ , stretching modes. The most essential difference in the phonon spectra is that the AlH<sub>4</sub> rotational modes ( $350$ – $580 \text{ cm}^{-1}$  in the  $\alpha$  phase) are softened substantially ( $200$ – $420 \text{ cm}^{-1}$ ) in the  $\gamma$  phase. This translates to an increase in vibrational entropy at temperatures for which these modes are active. We estimate the temperature-dependent free energy  $F(T)$  of the phases by adding the Bose-Einstein vibrational entropy contribution onto the ground-state

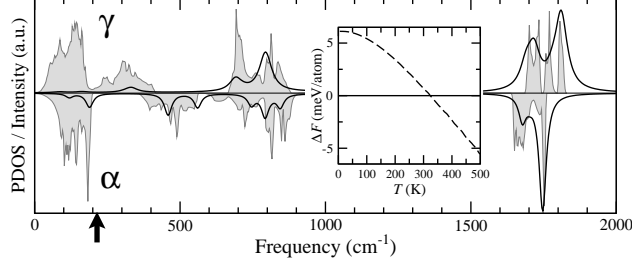


FIG. 3: Phonon density of states (grey shaded region) and Raman spectrum (solid black line, with thermal broadening) for  $\gamma$ - (top) and  $\alpha$ -NaAlH<sub>4</sub> (bottom). Raman peaks below 1000 cm<sup>-1</sup> are amplified tenfold for easier visibility. The arrow marks the the  $\alpha \rightarrow \gamma$  transition temperature. Inset shows the temperature dependence of the free-energy difference  $\Delta F = F_\gamma - F_\alpha$ .

total energy  $E_0$ :

$$F(T) = E_0 + \sum_{\mathbf{q},j} \left\{ \frac{1}{2} \hbar \omega_{\mathbf{q},j} + k_B T \ln \left[ 1 - \exp \left( -\frac{\hbar \omega_{\mathbf{q},j}}{k_B T} \right) \right] \right\}$$

where sums run over band indices  $j$  and wavevectors  $\mathbf{q}$  in the first Brillouin Zone. Neglecting further contributions to  $F(T)$ , we find good agreement between the transition temperature predicted by the free-energy analysis and that found in the dynamics simulations (250 K) when using identical simulation parameters. Upon increasing the plane-wave cutoff and including the Na semicore states to more accurately account for the zero-point motion as reported in Ref. 16, we obtain the results in Fig. 3, indicating a thermodynamic preference for the  $\gamma$  phase for  $T \geq 320$  K (see inset). Notably, this establishes the  $\gamma$  phase as the stablest variant within the experimental temperature range for dehydrogenation.

In a recent *in-situ* Raman study [32], Yukawa *et al.* found evidence of an unknown intermediate phase of NaAlH<sub>4</sub> in first-stage dehydrogenation, emerging in the uncatalyzed sample just before melting at 458 K. The authors suggest that, like our proposed  $\gamma$ -NaAlH<sub>4</sub>, this phase should be stable upon cooling to near room temperature and contain intact AlH<sub>4</sub> units with little constraint from the surrounding crystal lattice. Accordingly, we have calculated the Raman spectrum for  $\gamma$ -NaAlH<sub>4</sub>, shown in Fig. 3 [30]. A comparison between our results and the spectrum at 458 K in Ref. 32 shows a remarkable agreement between the two. Foremost, we note the new signature Al-H stretching peak near 1800 cm<sup>-1</sup> in both experiment and simulation. The simulations also record a second resonance at 1750 cm<sup>-1</sup>; although not explicitly visible in Ref. 32, asymmetry in their 1800 cm<sup>-1</sup> signature does suggest the pres-

ence of an additional lower-frequency peak. The difficulty in experimentally resolving these two peaks can be attributed to the thermally averaged nature of the finite-temperature  $\gamma$  structure with respect to its zero-temperature counterpart, as well as additional soft lattice modes activated during the transition (similar broadening is observable in the pair correlation data of Fig. 4). In the experiment, the 400–500  $\text{cm}^{-1}$  peaks disappear, and distinct peaks at 770 and 817  $\text{cm}^{-1}$  merge into a single broad peak. Both features are also visible in Fig. 3. Note that in reality, the 400–500  $\text{cm}^{-1}$  rotational modes in  $\alpha$ -NaAlH<sub>4</sub> do not disappear in  $\gamma$  but rather shift to a broad peak at  $\sim 300 \text{ cm}^{-1}$ ; however, the corresponding Raman-active peaks are too weak to demonstrate a resolvable signal. Collectively, these similarities present a strong case for the interpretation of the unknown phase in Ref. 32 as  $\gamma$ -NaAlH<sub>4</sub>.

A closer examination of the MD results elucidates why the  $\alpha \rightarrow \gamma$  transition is not observed in our bulk *NPT* simulations. In the surface slab simulations,  $\gamma$ -NaAlH<sub>4</sub> nucleated only upon activation of the rotational modes of surface AlH<sub>4</sub> units (center panel, Fig. 1a). This agrees with Fig. 3, since softening of AlH<sub>4</sub> rotational modes is the predominant contributor to the thermodynamic stability of the  $\gamma$  phase. However, in bulk  $\alpha$ -NaAlH<sub>4</sub> the AlH<sub>4</sub> units cannot rotate: the barrier to rotational mobility is larger than for the relatively unconstrained surface groups, and rotation must be coupled with large volume fluctuations. This makes ready nucleation of the  $\gamma$  phase in bulk NaAlH<sub>4</sub> difficult. Correspondingly, rotation of interior AlH<sub>4</sub> units in the (001) surface slab is strongly coupled to the volume expansion perpendicular to the surface. The calculated surface energy of  $\gamma$ -NaAlH<sub>4</sub>(001) is also much smaller than  $\alpha$ -NaAlH<sub>4</sub>(001) (3.1 versus 8.2 meV/ $\text{\AA}^2$ ), favoring the transition in the slab. The results show that AlH<sub>4</sub> rotation percolates once activated at the surface, as the slab thickness increases to accommodate. This lowers the barrier for *ab*-planar shear, finalizing the transition. We therefore assume that nucleation of  $\gamma$ -NaAlH<sub>4</sub> should occur more readily at an exposed (001) surface, at grain boundaries in a polycrystalline sample, or in low-stress regions that can accommodate the local volume fluctuations necessary for AlH<sub>4</sub> rotation.

We investigate the transition timescale in the MD simulations by introducing an order parameter  $\lambda$  as a reaction coordinate, defined as  $\lambda = 1 - f_{\text{edge}}/f_{\text{corner}}$ . Here  $f_{\text{edge}}$  and  $f_{\text{corner}}$  are the fractional occupancies of the edge-center and corner sublattices in the projection of the  $\alpha$  unit-cell geometry onto the surface plane (see Fig. 1b). The rapid evolution from  $\lambda = 0$  (i.e., pure  $\alpha$ ) to  $\lambda = 1$  (i.e., pure  $\gamma$ ) evidences the strong thermodynamic driving force

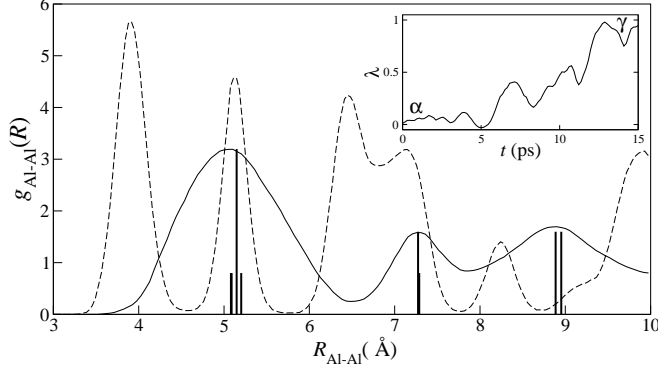


FIG. 4: Comparison of the Al–Al pair correlation function  $g_{\text{Al–Al}}$  for the (001) slab before (dashed line) and after (solid line) the  $\alpha \rightarrow \gamma$  transition at 275 K. Solid vertical lines give peak locations for a lattice-matched ideal crystal of  $\alpha\text{-Na}_3\text{AlH}_6$  (see text for definition), with relative peak heights shown for comparison. Inset shows the evolution of the order parameter  $\lambda$  during the transition.

for the transition (see inset, Fig. 4).

Geometric similarities in the aluminum substructures of  $\gamma\text{-NaAlH}_4$  and  $\alpha\text{-Na}_3\text{AlH}_6$  suggest a phenomenological connection between the  $\alpha \rightarrow \gamma$  transition and the  $\text{NaAlH}_4 \rightarrow \text{Na}_3\text{AlH}_6$  dehydrogenation reaction. These are quantified in Fig. 4, which compares the Al–Al pair correlation function for the (001) slab during the  $\alpha \rightarrow \gamma$  transition with one for  $\text{Na}_3\text{AlH}_6$  that is constrained to be lattice matched to the  $\gamma$  cell. Specifically,  $\alpha\text{-Na}_3\text{AlH}_6$  peaks were obtained by isotropically shrinking the cell volume (-10%) to match the mean lattice parameter in the  $ab$  plane to the  $\gamma\text{-NaAlH}_4$  cell boundaries. The striking agreement between the locations and relative heights of the two sets of peaks strongly hints at the role of  $\gamma\text{-NaAlH}_4$  as a key intermediate during dehydrogenation. If so, the role of exposed surfaces in nucleating  $\gamma$  may help to account for the enhancement of dehydrogenation kinetics due to ball milling without a catalyst [33], as well as improved kinetics of  $\text{NaAlH}_4$  nanoparticles [34]. We did not examine the impact of transition metal additives; however, the catalyst is likely to further aid the conversion of  $\gamma\text{-NaAlH}_4$  to  $\alpha\text{-Na}_3\text{AlH}_6$ . A detailed investigation of this possibility is currently underway.

In conclusion, we have discovered and characterized a new phase of  $\text{NaAlH}_4$ , labeled here as  $\gamma$ . Our description is fully consistent with an unknown intermediate found in a recent *in-situ* Raman study. Activation of the  $\text{AlH}_4$  rotational modes drives the transition to  $\gamma$ , which occurs readily in (001) surface slab simulations for  $T \geq 320$  K. The thermodynamic

stability of  $\gamma$ -NaAlH<sub>4</sub> beyond this temperature has been further confirmed by vibrational entropy calculations using density-functional perturbation theory. Remarkable structural similarities between  $\gamma$ -NaAlH<sub>4</sub> and  $\alpha$ -Na<sub>3</sub>AlH<sub>6</sub> suggest that the  $\gamma$  phase should play a key role in mediating dehydrogenation. Notably, no Al–H bonds were broken in our simulations; this agrees with Ref. 35 and underscores the need for an additional defect-driven mechanism to fully account for dehydrogenation. Accordingly, further investigation of low-energy defects in  $\gamma$ -NaAlH<sub>4</sub> that could facilitate Al–H cleavage is recommended.

Funding was provided by DOE via CSGF and Hydrogen Program DE-FG02-05ER46253. Calculations were performed using Quantum-Espresso [21] on facilities provided through NSF Grant DMR-0414849. The authors thank Gerbrand Ceder for helpful discussions, and Elise Li for the quantum-chemistry results.

- 
- [1] L. Schlapbach and A. Züttel, *Nature* **414**, 353 (2001).
  - [2] B. Bogdanović and M. Schwickardi, *J. Alloys Comp.* **253&254**, 1 (1997).
  - [3] F. Schüth, B. Bogdanović, and M. Felderhoff, *Chem. Commun.*, 2249 (2004).
  - [4] M. E. Arroyo y de Dompablo and G. Ceder, *J. Alloys Comp.* **364**, 6 (2004).
  - [5] A. Peles *et al.*, *Phys. Rev. B* **70**, 165105 (2004).
  - [6] A. Aguayo and D. J. Singh, *Phys. Rev. B* **69**, 155103 (2004).
  - [7] J. Íñiguez *et al.*, *Phys. Rev. B* **70**, 060101 (2004).
  - [8] V. Ozoliņš, E. H. Majzoub, and T. J. Udovic, *J. Alloys Comp.* **375**, 1 (2004).
  - [9] C. Moysés Araújo *et al.*, *Phys. Rev. B* **72**, 165101 (2005).
  - [10] O. M. Løvvik and S. M. Opalka, *Phys. Rev. B* **71**, 054103 (2005).
  - [11] X. Ke and I. Tanaka, *Phys. Rev. B* **71**, 024117 (2005).
  - [12] T. Vegge, *Phys. Chem. Chem. Phys.* **8**, 4853 (2006).
  - [13] S. Li, P. Jena, and R. Ahuja, *Phys. Rev. B* **73**, 214107 (2006).
  - [14] T. J. Frankcombe and O. M. Løvvik, *J. Phys. Chem. B* **110**, 622 (2006).
  - [15] A. Marashdeh *et al.*, *Chem. Phys. Lett.* **426**, 180 (2006).
  - [16] A. Peles and M. Y. Chou, *Phys. Rev. B* **73**, 184302 (2006).
  - [17] A. J. Du, S. C. Smith, and G. Q. Lu, *Appl. Phys. Lett.* **90**, 143119 (2007).
  - [18] A. Peles and C. G. Van de Walle, *Phys. Rev. B* **76**, 214101 (2007).

- [19] J. Íñiguez and T. Yildirim, J. Phys. Cond. Matt. **19**, 176007 (2007); Appl. Phys. Lett. **86**, 103109 (2005).
- [20] H. Gunaydin, K. N. Houk, and V. Ozoliņš, PNAS **105**, 3673 (2008).
- [21] P. Giannozzi *et al.*, J. Phys. Condens. Matt. **21**, 395502 (2009).
- [22] J. P. Perdew, K. Burke, and M. Ernzerhof, Phys. Rev. Lett. **77**, 3865 (1996).
- [23] D. Vanderbilt, Phys. Rev. B **41**, 7892 (1990).
- [24] N. Troullier and J. L. Martins, Phys. Rev. B **43**, 1993 (1991).
- [25] S. G. Louie, S. Froyen, and M. L. Cohen, Phys. Rev. B **26**, 1738 (1982).
- [26] R. Car and M. Parrinello, Phys. Rev. Lett. **55**, 2471 (1985).
- [27] P. Focher *et al.*, Europhys. Lett. **26**, 345 (1994).
- [28] G. J. Martyna, M. L. Klein, and M. E. Tuckerman, J. Chem. Phys. **97**, 2635 (1992).
- [29] R. S. Kumar *et al.*, Phys. Rev. B **75**, 174110 (2007).
- [30] See EPAPS Document No. ??? for list of Raman peak locations and for full phonon and XRD spectra.
- [31] S. Baroni, S. de Gironcoli, and A. D. Corso, Rev. Mod. Phys. **73**, 515 (2001).
- [32] H. Yukawa *et al.*, J. Alloys Comp. **446-447**, 242 (2007).
- [33] D. L. Anton, J. Alloys Comp. **356-357**, 400 (2003).
- [34] S. Zheng *et al.*, Chem. Mater. **20**, 3954 (2008).
- [35] E. H. Majzoub, K. F. McCarty, and V. Ozoliņš, Phys. Rev. B **71**, 024118 (2005).